Pergamon

0148-9062(94)00012-3

Int. J. Rock Mech. Min. Sci. & Geomech. Abstr. Vol. 31, No. 6, pp. 643–659, 1994

0148-9062/94 $7.00 + 0.00

The Progressive Fracture of Lac du Bonnet Granite

C. D. MARTIN†
N. A. CHANDLER†

The strength of intact rock is made up of two components: the intrinsic strength, or cohesion; and the frictional strength. It is generally assumed that cohesion and friction are mobilized at the same displacements such that both components can be relied on simultaneously. Damage testing of samples of Lac du Bonnet granite has shown that as friction is mobilized in the sample, cohesion is reduced. This progressive loss of intrinsic strength and mobilization of friction is modelled using the Griffith locus based on a sliding-crack model. There appears to be a maximum cohesion that can be relied on for engineering purposes, and this strength is less than half of the unconfined compressive strength measured in the laboratory.

INTRODUCTION

The progressive failure of clays and soft rocks is a well-known phenomenon involving a loss of cohesive strength [1]. In brittle rocks, however, progressive failure is not generally recognized. It is obvious though that the strength loss when progressing from an intact rock through to a jointed rock mass must also be related to a loss in cohesion, or intrinsic strength.

In many engineering applications, particularly at shallow depths, jointed rock masses are the norm, and the rock-mass strength, after sufficient deformation, is essentially frictional resistance. However, in the mining, petroleum and nuclear industries, excavations are being made at ever increasing depths where large volumes of essentially intact rock, i.e. tightly interlocked rock mass, are being encountered. In these situations stresses are generally much higher, and the cohesion component of the failure envelope plays a major role in determining the stability around underground openings.

The strength of intact rock is made up of two components, cohesion and friction. For engineering purposes it is often assumed that these components of intact strength are mobilized at the same displacements such that both components can be relied on simultaneously. The strength of intact rock is determined using laboratory triaxial tests, and the sum of the cohesion and friction components is obtained from these tests. In an effort to understand the progressive failure of intact rock, a series of damage-controlled tests has been carried out on samples of Lac du Bonnet granite.

†AECL Research, Whiteshell Laboratories, Pinawa, Manitoba, Canada R0E 1L0.

LABORATORY DEFINED PARAMETERS

Testing procedures for determining the compressive deformational behaviour of rock samples are given by ISRM [2]. These include recording the axial (ϵ_{axial}) and lateral ($\epsilon_{lateral}$) strains in a sample as it is loaded with or without a fixed confining stress. Richart *et al.* [3], in 1928, first noted that volumetric strain, in addition to the axial and lateral strains, was also an important measurement in compression testing, and Cook [4] proved that the volumetric strain of a sample measured by surface strain gauges was a pervasive volumetric property of the rock and not a superficial phenomenon. For a cylindrical sample subjected to axial loading, with or without a confining stress, and under small strains, the volumetric strain (ϵ_v or $\frac{\Delta V}{V}$) is given by:

$$\epsilon_v = \frac{\Delta V}{V} \simeq \epsilon_{axial} + 2\epsilon_{lateral}. \quad (1)$$

Hence by plotting the axial, lateral and the calculated volumetric strains versus the applied axial stress, the path of a rock sample to failure can be followed. An example of axial, lateral and volumetric strain versus axial stress curves for Lac du Bonnet granite in uniaxial compression is given in Fig. 1.

The failure of brittle rocks has been investigated by many researchers [5–14]. These researchers showed that the stress–strain curves for a brittle material can be divided into five regions (Fig. 1). The initial region of the stress–strain curves in Fig. 1 represents the closure of existing microcracks in the sample and may or may not be present, depending on the initial crack density and crack geometry. Once the existing cracks are closed, then the rock is presumed to be a linear, homogeneous,

elastic, material (Region II). The elastic properties of a rock sample can be determined from this portion of the stress–strain curves.

The onset of dilation marks the beginning of Region III. Brace *et al.* [6] found that dilation begins at a stress level of about 30–50% of the peak strength. It is worth noting that this dilation is only registered on the lateral strain gauge and must therefore reflect the growth of axial cracks, i.e. cracks parallel to the direction of the maximum applied load. Hence this stress level will be referred to as the crack-initiation stress (σ_{ci}). These cracks are generally thought of as stable cracks since an increase in load is required to cause further cracking. Crack initiation is difficult to identify from the laboratory stress–strain curves, particularly if the sample already contains a high density of microcracks. The crack-initiation stress is best determined using a plot of crack volumetric strain versus axial strain. Crack volumetric strain is calculated as follows. First the elastic volumetric strains are calculated using the elastic constants (E, ν) from the linear portion of stress–strain curves in Region II by

$$\Delta V/V_{\text{elastic}} = \frac{1-2\nu}{E}(\sigma_1 - \sigma_3) \qquad (2)$$

The elastic volumetric strains are subtracted from the total measured volumetric strains to determine the volumetric strains caused by the axial cracking (Fig. 1). σ_{ci} is the axial stress at which dilation just begins on the crack-volume plot, as shown in Fig. 1. Researchers [7, 5, 15] have found that the cracking associated with axial stresses slightly above σ_{ci} does not result in reduced rock strength. Therefore these random stable axial cracks are not considered damaging to the rock strength in laboratory tests.

The axial stress level where the total volumetric strain reversal occurs marks the beginning of Region IV and represents the onset of unstable crack growth, as defined by Bienawaski [7]. It generally occurs at axial stress level between 70 and 85% of the short-term peak strength. It is at this stress level that the axial strain departs from linearity (Fig. 1). The dominant mechanism resulting in such an increase in axial strains is sliding along inclined surfaces. Hallbauer *et al.* [13] pointed out that this region is characterized by the most significant structural changes to the sample, with the density of microcracks increasing by about sevenfold. This stress level has particular significance in the concrete industry as it is used to establish the long-term strength of concrete

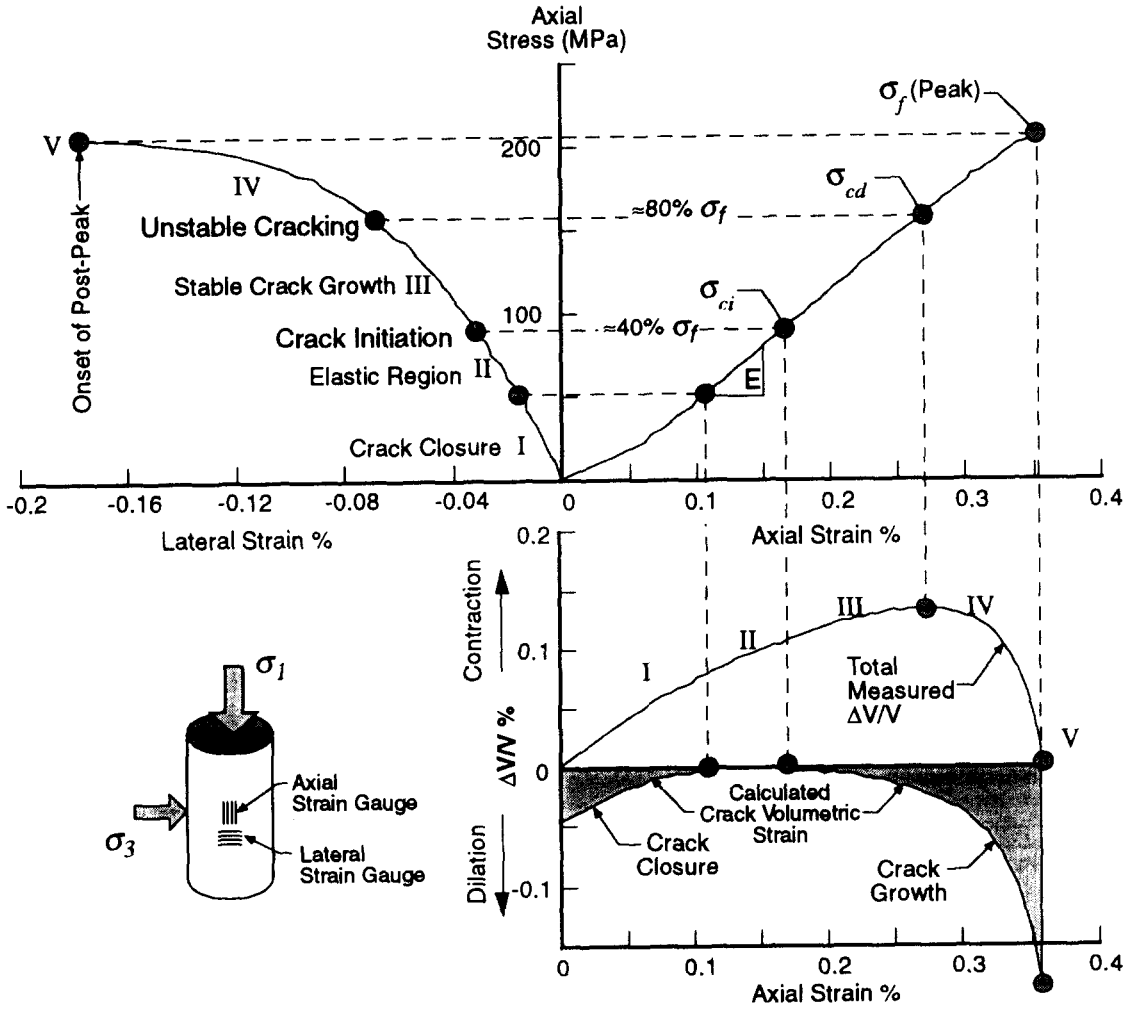

Fig. 1. Stress–strain diagram obtained from a single uniaxial compression test for Lac du Bonnet granite showing the definition of crack initiation (σ_{ci}), crack damage (σ_{cd}) and peak strength. Note only the axial and lateral strains are measured. The volumetric strain and crack volumetric strain are calculated.

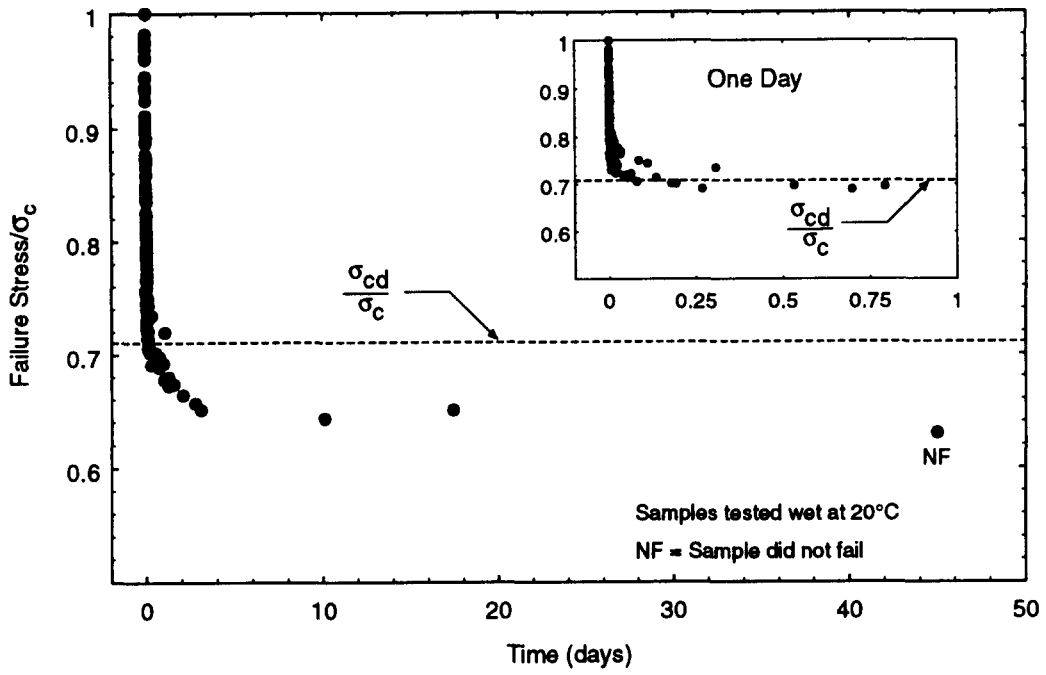

Fig. 2. The strength of unconfined samples of Lac du Bonnet granite subjected to long-term constant load. σ_c is the standard short-term unconfined compressive strength.

[16, 17, 18]. Lajtai *et al.* [19] found that the unstable crack stress for unconfined samples of Lac du Bonnet granite from the Cold Spring Quarry occurred at 70% of the short-term peak strength. Schmidtke and Lajtai [20] did extensive long-term testing of Lac du Bonnet granite from Cold Spring Quarry. Their results were reanalysed by the authors and have been replotted in Fig. 2. Figure 2 shows that for loads above ≈ 0.70 of the peak strength (σ_c), failure occurs almost immediately. Thus the increase in load above the unstable crack stress is a temporary strain-hardening effect that cannot be relied on for permanent loading conditions. Hence, we will refer to this stress level as the crack-damage stress (σ_{cd}) since loads above this stress level result in damage to the material which cannot be tolerated under a permanent load.

The peak strength of the material (σ_f) marks the beginning of post-peak behaviour, Region V, and is almost universally used to establish the failure strength envelope. An example of the complete axial stress–strain curves for Lac du Bonnet granite is shown in Fig. 7. Beyond the peak, the axial stress versus axial strain shows a rapid decrease, which is interrupted by one or more short strengthening interludes, marked by steps in the descending axial stress curve. Lockner *et al.* [21] reported that during the first portion of the post-peak axial stress versus axial strain descent, the loci of the seismic events indicated the development of a major inclined shear fracture.

Thus far, three characteristic stress levels have been identified in the laboratory stress–strain curves (see Fig. 1): the crack-initiation stress (σ_{ci}), caused by stable tensile cracking; the crack-damage stress (σ_{cd}), caused by crack sliding; and the peak strength (σ_f). In order to better understand material behaviour, it is important to establish which of these stress levels are characteristic material parameters and which are a function of the particular loading conditions used in the uniaxial test. Hudson *et al.* [22] concluded that the peak strength of a sample was a function of the boundary conditions of the test, and hence not an inherent material property.

Glucklich and Cohen [23, 24] used stored strain energy to explain peak-strength scale effects, which are commonly observed. They point out that, during the stage of stable crack growth, there is equilibrium between the external load and the crack length. This was also confirmed by Hoek and Bieniawski [5]. Both the loads and the stable crack lengths increase up to the critical moment at which the strain-energy release rate equals or exceeds that of energy absorption. At this moment crack propagation becomes unstable, and the material reaches its peak strength. For heterogeneous materials such as rock, the propagating crack will most likely encounter material that is stronger or weaker (an area of pre-existing stable cracks) than the mean strength. In either case, after the propagating crack advances through the softer or harder material, there is an excess of energy released that is converted to kinetic energy and is available to do work against the remaining uncracked material. It is here that the volume of the sample and the stiffness of the testing machine play a critical role because the stored energy in the total system dictates the energy release rate. In essence, Glucklich and Cohen are pointing out that a properly conducted compressive-strength test would balance the stored strain energy in the sample and loading frame with the fracture surface energy required for fracture growth, i.e. there would be no kinetic energy available to propagate the crack. In reality this is very difficult to do because in compression testing two modes of cracking are developing simultaneously, the axial crack and the sliding crack. One approach to this problem is to reduce the loading rate such that

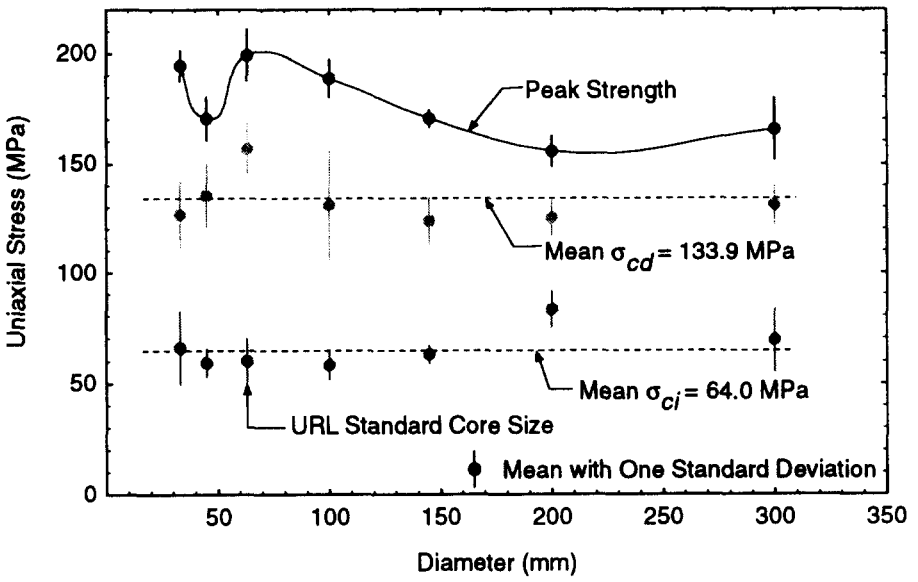

Fig. 3. The effect of sample diameter on peak strength, crack-damage stress and crack-initiation stress of 53 samples of Lac du Bonnet granite from the 240 Level of the Underground Research Laboratory.

the fracture surface has time to grow and increase the sample volume to minimize the effect of heterogeneity on the fracture process. A similar approach is used to reduce strain-hardening effects in more ductile materials [25].

The long-term test data of Schmidtke and Lajtai [20] (see Fig. 2) also suggest that the peak load above the crack-damage stress is only sustained by the rock for a short duration and cannot be relied on for the long term. This leaves only σ_{ci} and σ_{cd} as possible material parameters that should therefore be independent of sample volume.

To determine the effect of scale on σ_{cd} and σ_{ci}, the stress–strain curves were analysed for 53 samples, with diameters ranging from 33 to 300 mm diameter. The results are summarized in Fig. 3, and the peak strength is shown for comparison. The peak strength, as expected, shows a modest reduction in strength for larger samples, but both σ_{ci} and σ_{cd} appear to be unaffected by sample volume. Note that except for the largest sample diameter tested, the data suggest that the peak strength is trending towards the σ_{cd} strength, i.e. about 70% of the peak strength. This result is in keeping with that of Hoek and Brown [26], who showed the unconfined compressive strength reducing to about 80% of the peak strength of a small sample, as the sample diameter increased from 10 to 200 mm.

In an effort to minimize the potential influence of uncontrolled strain energy on the test results, one final series of tests was carried out that attempted to combine the effects of scale and a slow loading rate. Four 200-mm-diameter samples were tested at the loading rate of 0.00075 MPa/sec, which is 1000 times slower then the normal loading rate. In two samples, failure occurred at the stress level generally associated with σ_{cd}, and those samples did not display the normal volumetric strain reversal (Fig. 4). Interestingly, the samples that were subjected to slow loading rates all developed characteristic shear planes not generally associated with unconfined testing (Fig. 5). This also concurs with the previously mentioned notion that the failure mechanism for σ_{cd} is one of sliding. It would appear that with the appropriate boundary conditions, i.e. loading rate, loading-frame stiffness and sample volume, the peak strength of a sample of Lac du Bonnet granite would

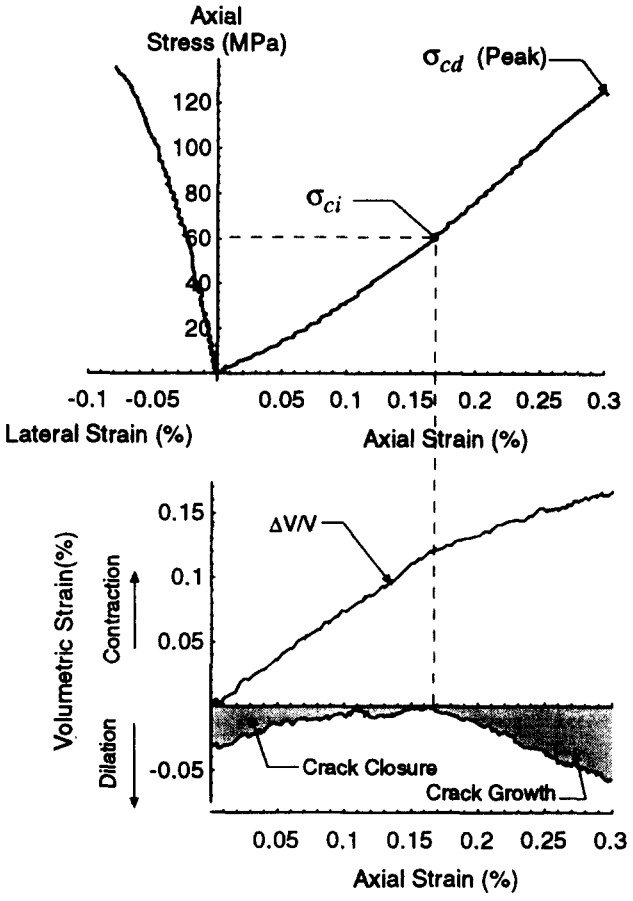

Fig. 4. The combined effect of sample diameter (200 mm) and slow loading (0.00075 MPa/sec) on peak strength, crack-damage stress and crack-initiation stress. In this sample the crack-damage stress is the peak strength.

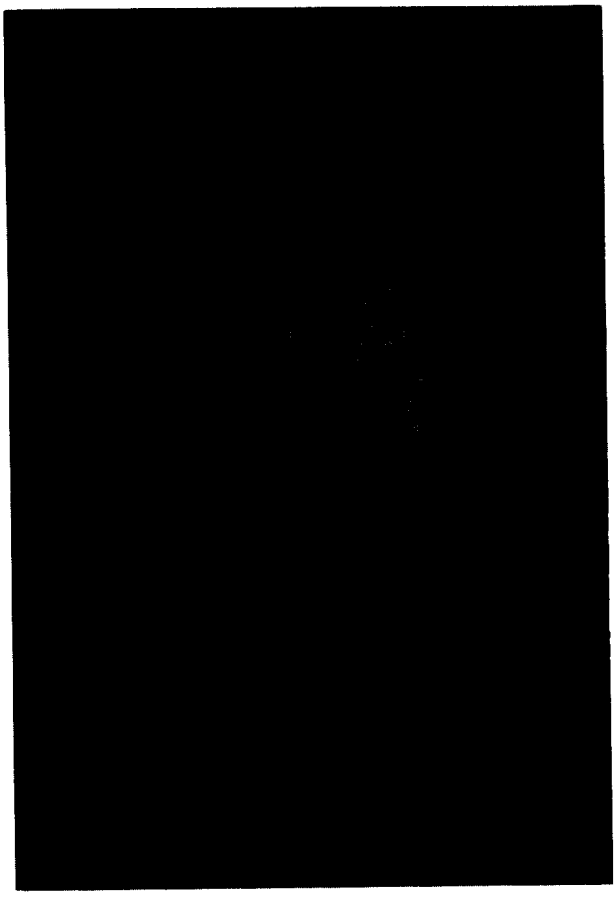

Fig. 5. The failure surface, developed in a sample subjected to 0.00075 MPa/sec loading rate, is inclined 23° with respect to the direction of loading. Note the short axial cracks that form adjacent to the failure surface.

be reduced to about 80% of the standard uniaxial strength (σ_c), similar to the failure loads of Schmidtke and Lajtai [20].

Having established that σ_{cd} is the true peak strength of a rock in a monotonically loaded uniaxial compression test and that σ_{cd} and σ_{ci} are scale-independent parameters with completely different modes of origin, the next step is to determine the effect of increasing crack damage in a specimen on these two parameters.

DAMAGE-CONTROLLED TESTING

The Lac du Bonnet granite is medium to coarse grained and composed of approx. 30% K-feldspar, 30% plagioclase, 30% quartz and 10% mafic minerals, mainly biotite. The average grain size of the medium-grained granite is about 3–4 mm. Six post-failure uniaxial compression tests and thirty-one post-failure triaxial compression tests were conducted on the 63-mm-diameter grey samples. The samples were obtained from the 420 Level of AECL's Underground Research Laboratory.

The testing was carried out by CANMET (Canada Centre for Mineral and Energy Technology) [27], and specimens were prepared in accordance with the methods suggested by the International Society for Rock Mechanics [2]. The post-failure tests were conducted using an MTS 815 Rock Test System, a computer-controlled, servo-hydraulic compression machine, consisting of a 2.22 MN rated load cell, load frame, hydraulic power supply, triaxial cell, confining pressure subsystem, test controller, test processor and DEC micro PDP 11/73 computer. The triaxial cell is equipped with three linear variable differential transformers (LVDT) for the measurement of axial strain and a circumferential extensometer to measure the lateral strain.

The confining pressure and the axial stress were initially increased from zero to the required confining stress at the rate of 0.75 MPa/sec. The axial stress was then increased using axial strain-rate control at a rate approximating 0.75 MPa/sec. The instrumentation was scanned every 3 sec. Up to approx. 75% of the expected peak strength, the load–unload cycles were carried out at 40 MPa increments. As the peak strength of the sample was approached, special care was taken to prevent rapid failure in order to continue the test into the post-failure region. After the axial stress reached $\approx 75\%$ of the expected peak strength, the load–unload cycles were performed at 0.063 mm increments of circumferential deformation using axial-strain control. A test took about 8 hr to complete, and a typical result is shown in Fig. 6.

The initial concern was whether the testing method influenced the results. Figure 7 compares the results from an unconfined damage-controlled test with a traditional unconfined post-failure test without the damage increments. Figure 7 illustrates that the general shape of the stress–strain plot, particularly in the prepeak region, is unaffected by the testing method. This was also found true for the confined tests.

TEST RESULTS

The purpose of the testing was to determine the effect of damage on the stress levels associated with crack initiation and crack damage. The volumetric strain encompasses both the damage in the lateral and axial direction and can be related to crack-initiation and crack-damage stress (see Fig. 1). In a given test, a damage increment (i), i.e. a load–unload cycle, will produce permanent volumetric damage (ϵ_v^p). A damage parameter (ω) is therefore defined as the cumulated permanent volumetric strain (Fig. 8)

$$\omega = \sum_{i=1}^{n} (\epsilon_v^p)_i \%. \tag{3}$$

It is useful to plot the peak stress, σ_{cd} and σ_{ci}, versus the damage parameter ω. The collection of these values of peak stress, σ_{cd} and σ_{ci}, for any one test will be referred to as the peak (ω) locus, the σ_{cd} locus and the σ_{ci} locus.

Crack initiation and crack damage

The crack-initiation stress occurs when the load first exceeds about 0.2–0.4 of the peak strength. Initially, in the early stages of the test, the crack-initiation stress appears to increase slightly, however, as damage accumulates the slope of the crack initiation locus appears to level off. One could speculate that the initial increase

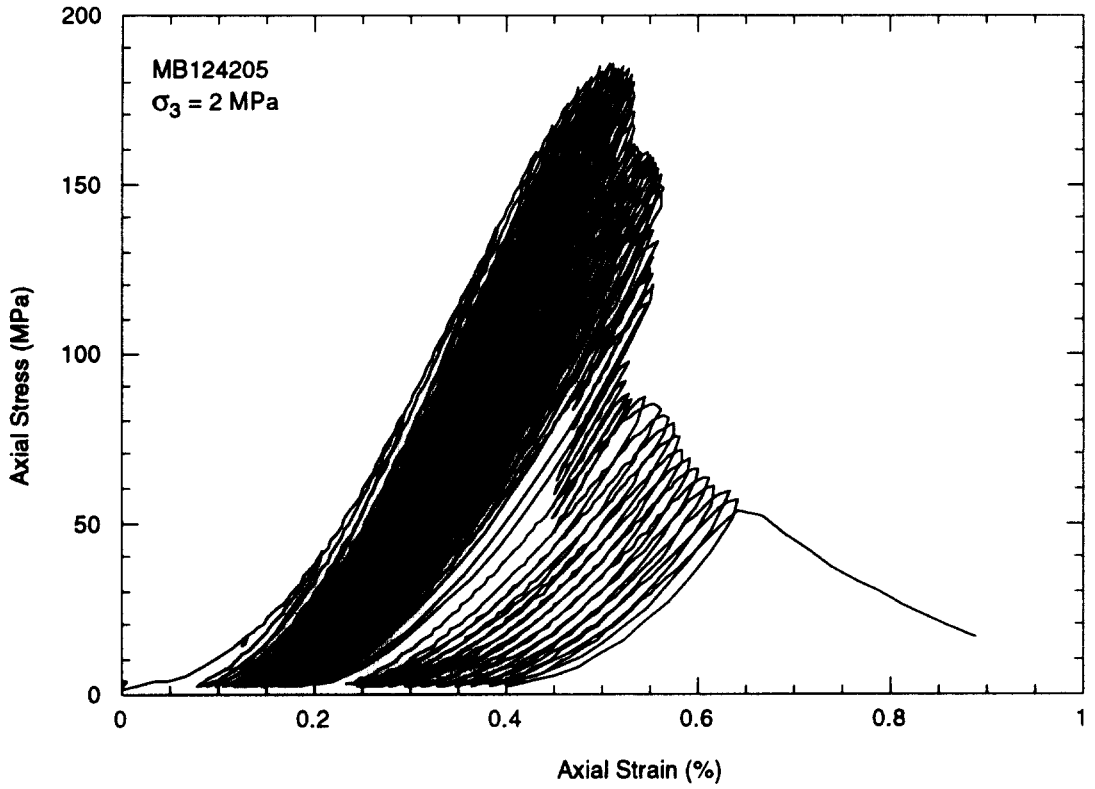

Fig. 6. Example of the repeated loading and unloading used in a damage-controlled test.

in the σ_{ci} locus is related to less critical cracks requiring more load to reach crack initiation. Given the difficulty in determining the σ_{ci} stress in the early stages of the test, it may be that the initial σ_{ci} slope is within the error of the analysis. Also, this phenomenon was not observed in all the test results. Thus it is reasonable to conclude that the crack-initiation locus remains fairly constant with each damage increment and is therefore independent of the damage accumulated in the sample (Fig. 9).

The crack-damage stress occurs at about 0.8 of the peak strength. However, unlike the crack-initiation stress, the crack-damage stress reduces significantly in the early stages of the test and reaches a threshold as the damage accumulates in the sample (Fig. 9). This phenomenon is seen at all confining stress levels and is

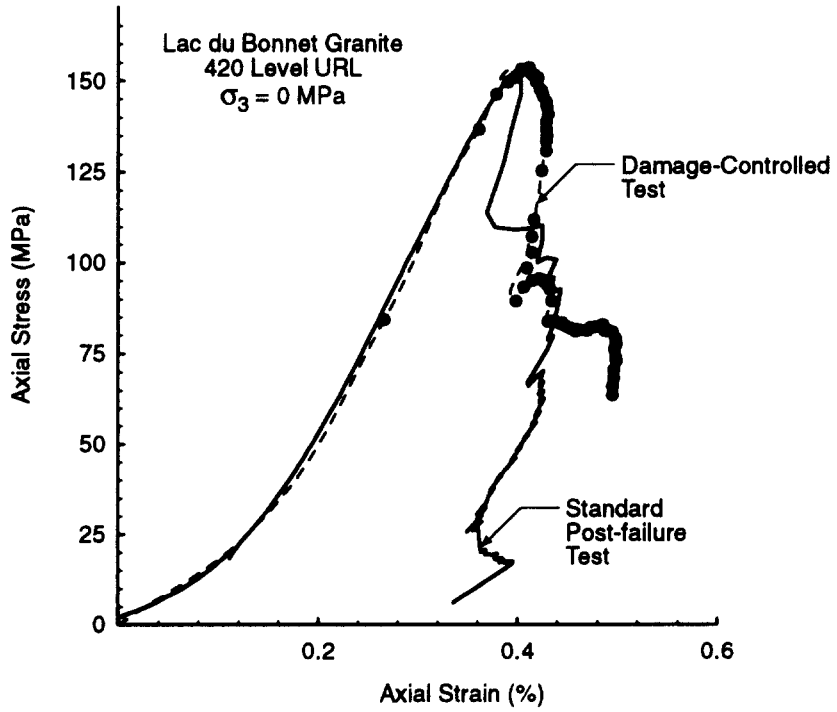

Fig. 7. Comparison of an unconfined damage-controlled test and a standard unconfined post-failure test.

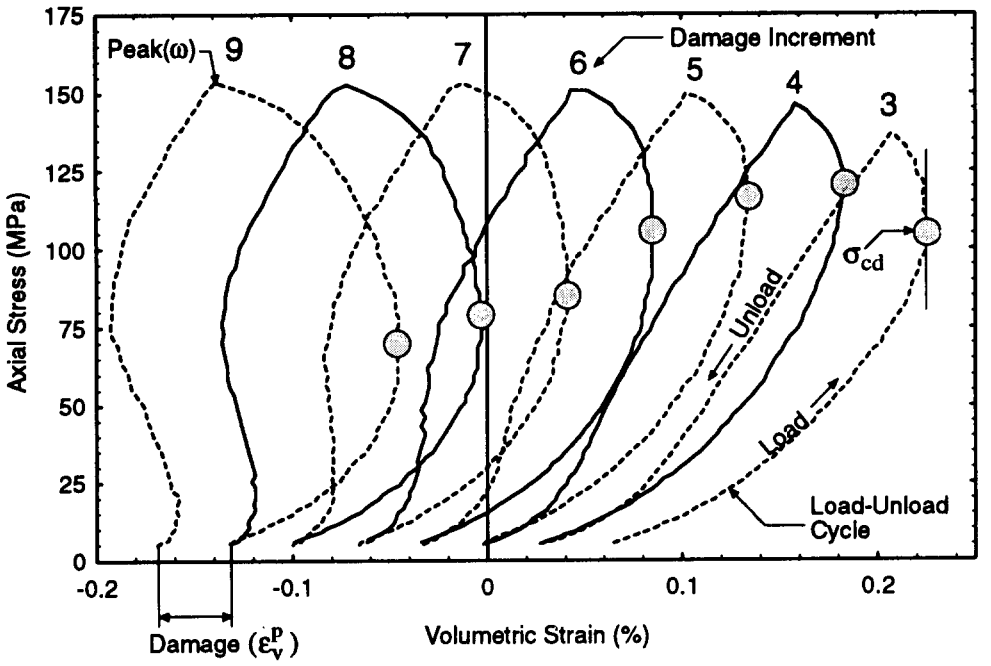

Fig. 8. Damage is defined as the permanent volumetric strain resulting from a single damage increment.

quite consistent from test to test (Fig. 10). Similar observations [28,29,30] have been made during the cyclic testing of other brittle rocks. It should be noted that the drop in σ_{cd} is smaller at higher confining stresses and that the threshold value of σ_{cd} corresponds approximately to σ_{ci} when the sample is unconfined. As the confining stress is increased, the threshold value of σ_{cd} is greater than σ_{ci} (Fig. 11).

Deformation constants

Young's modulus and Poisson's ratio can be determined for each damage increment. Each increment is treated as a separate test, and the modulus and Poisson's ratio are computed for the part of the stress–strain curve that lies between the crack-closure stress and the crack-initiation stress. A plot of Young's modulus and Poisson's ratio versus damage is compared with the crack-damage locus in Fig. 12. As the sample is subjected to increasing damage, a gradual reduction in stiffness is indicated (Fig. 12). In the post-peak region of the test in which the peak (ω) stress dropped from about 150 to 56 MPa ($\approx$35% of maximum value), the modulus decreased from 50 to 24 GPa ($\approx$50% of maximum value). At a confining pressure greater than 20 MPa, the

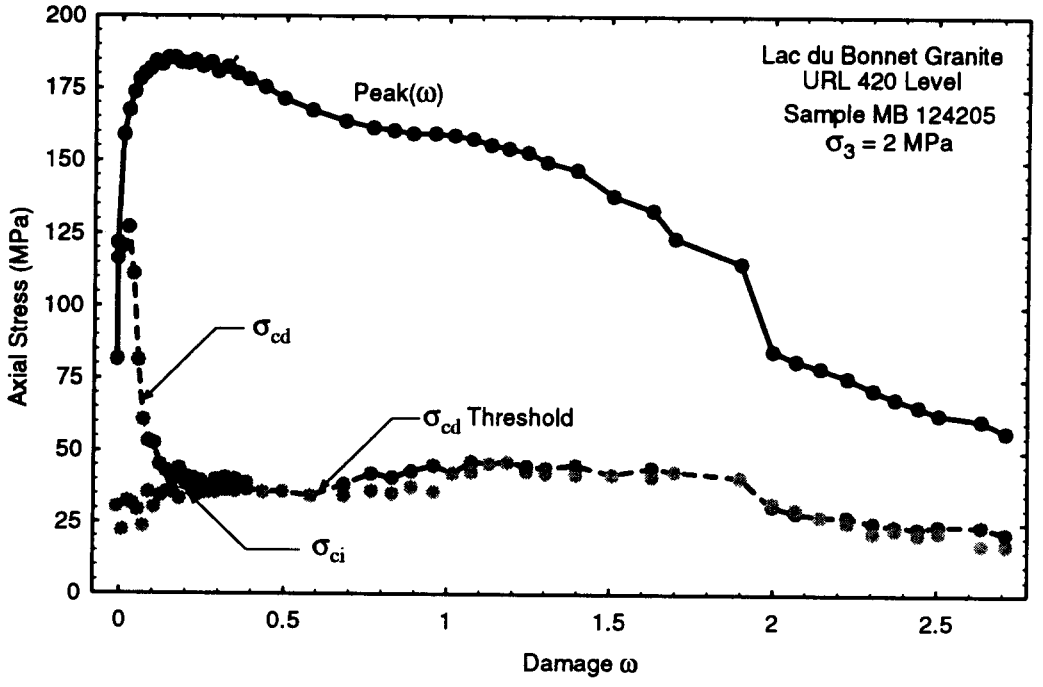

Fig. 9. Example of the crack-initiation stress and the crack-damage stress as a function of damage. Note that at low confining stresses, the crack-damage stress is essentially the same magnitude as the crack-initiation stress.

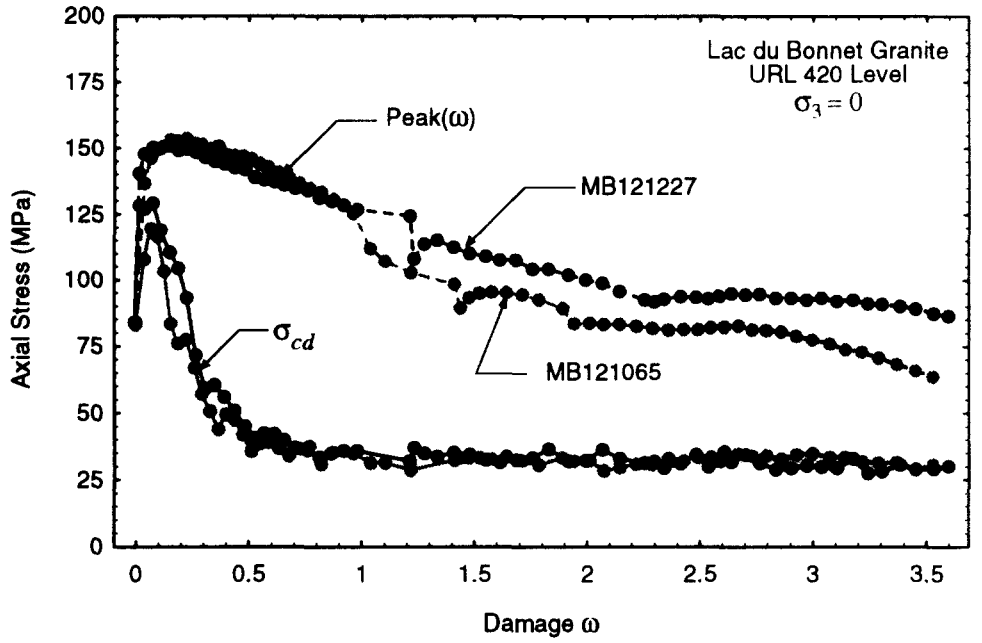

Fig. 10. Unconfined example of the crack-damage stress and the peak stress as a function of damage. Note the repeatability between tests.

reduction in the modulus in the post-peak regime was considerably less. In all cases, the strength reduced faster than the modulus.

In the early portion of testing, i.e. before σ_{cd} is reached, Poisson's ratio is about 0.14 and increases to about 0.2 at the maximum σ_{cd} (Fig. 12). As the peak (ω) stress level exceeds the initial σ_{cd} and starts its descent to the post-peak strength, Poisson's ratio increases quite sharply to about 0.9. It is obvious that above 0.5 this ratio is only relating lateral strains to axial strains and is not an elastic constant. As the σ_{cd} threshold is reached and after the initial large drop in the post-peak strength, the ratio remains relatively high, ranging from 0.6 to 0.9. The locus of Poisson's ratio clearly establishes that two phases of axial crack growth occurs. The first phase occurs in the pre-peak portion of the test when the ratio is increasing quite rapidly, indicating significant axial crack growth. The second phase occurs when the sample enters into the post-peak region and the first significant strength drop occurs. This phase is indicative of when the sample has developed a major shear fracture as identified by Lockner *et al.* [21].

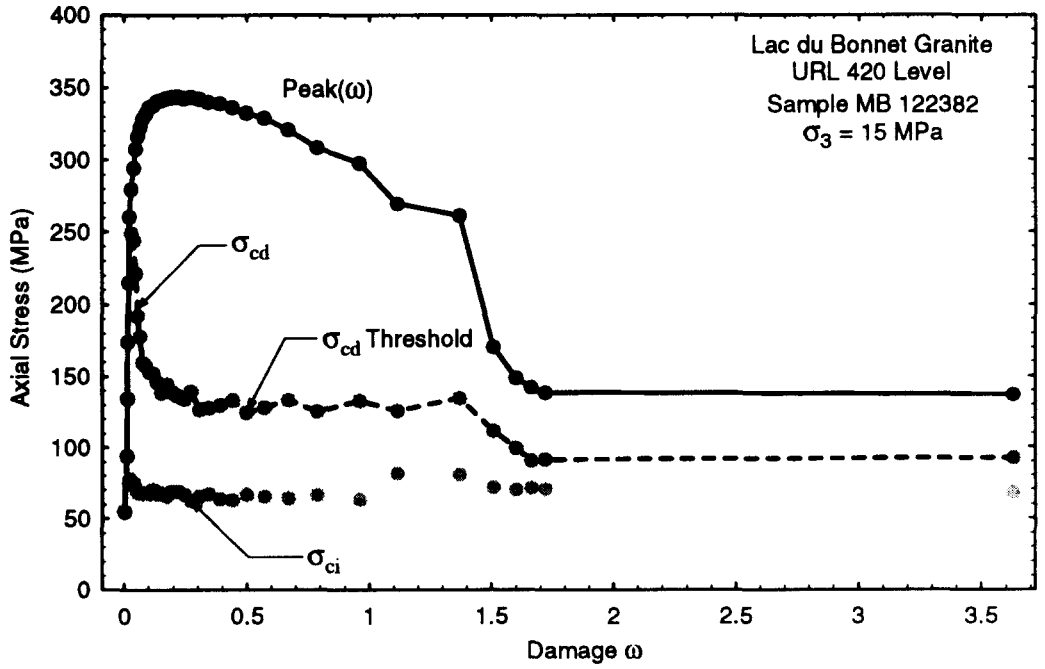

Fig. 11. Confined example of the crack-initiation stress and the crack-damage stress as a function of damage. Note that at higher confining stresses, the crack-damage stress is considerably higher than the crack-initiation stress.

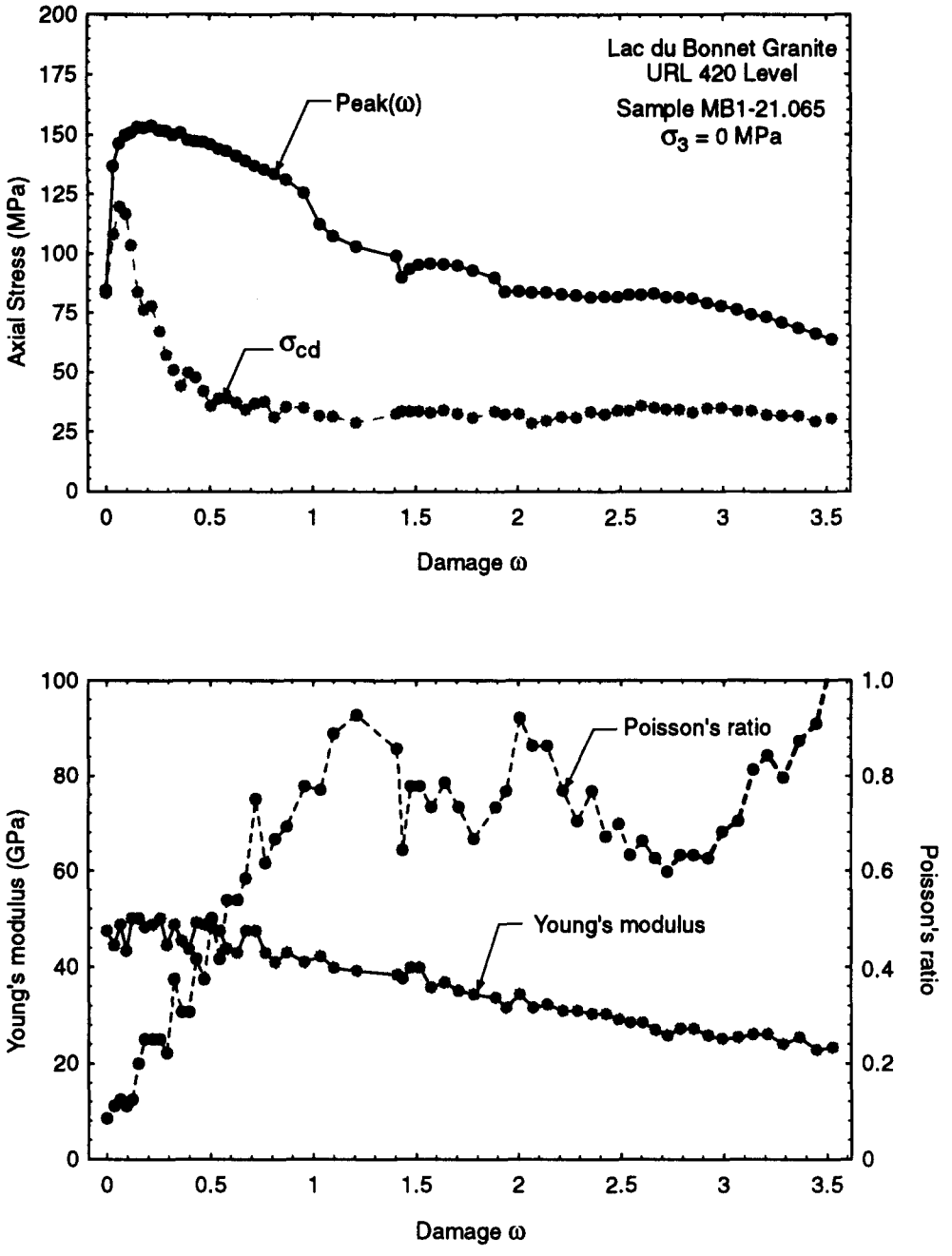

Fig. 12. Modulus and Poisson's ratio as a function of damage.

CRACK DAMAGE LOCUS

The theoretical limit of crack growth for brittle materials has been evaluated by Berry [31,32] for tensile crack extension, and by Cook [33] for shear crack extension. Cook [33] refers to this limit for crack growth as the Griffith locus, and it follows the general form ABCD, given in Fig. 13. According to Berry, the Griffith locus can be interpreted in the following way. The portion AB, during the early stages of crack extension, indicates a rapid loss in strength with no increase in axial strain. Unless the strain energy released from the elastically strained regions around the propagating crack is removed from the system, the excess energy will be converted to kinetic energy. It is generally not possible to follow the unloading path AB since most systems, even a stiff testing apparatus, have a finite unloading stiffness, represented by AC in Fig. 13. Thus a crack starting at σ_A will propagate dynamically†. Berry [31] noted that the excess strain energy represented by the shaded area ABC will cause the crack growth to accelerate, hence the crack will continue to extend even as the stress drops below σ_C corresponding to point C on the failure locus. Below σ_C the crack will finally stabilize when the excess strain energy ABC is equal to the strain energy CDE. The area ABC = CDE, and hence the energy CDE, is the surface energy required to create longer cracks. The longer crack is now represented by OD, with a reduced modulus E_{c+dc}. These cracks are now loaded to a subcritical stress level σ_E, and hence will

†In a servo-controlled laboratory test the energy that causes the dynamic propagation is controlled. Hence, it is possible to follow this stage of crack growth.

not extend until the stress level is increased to σ_D. Thus the Griffith locus has two key elements: the stiffness of the initial material which controls the position of OA; and the crack properties that control the shape and position of BCD (see Fig. 13).

Thus far the crack damage locus has been plotted versus the damage parameter ω, which is defined by the volumetric strain. Although σ_{cd} is defined by the volumetric strain reversal, it also corresponds to the onset of nonlinearity in the axial stress versus axial strain plot, as shown in Fig. 1. Earlier it was suggested that this non-linear response is a direct result of sliding along crack surfaces angled with respect to the direction of the maximum load. Thus it is instructive to replot the test results to see the relationship between the crack damage locus and the peak (ω) stress versus axial strain. Figure 14 shows a typical plot of the crack-damage locus and peak (ω) stress locus versus axial strain. The volumetric strain versus axial strain is also shown to illustrate how the plot is generated. Note that the full reduction in σ_{cd} to its threshold level occurs by damage increment 10, which takes place before the peak strength of the sample is reached. This was not evident from the previously presented plots. The shape of the damage locus on an axial stress versus axial strain plot is similar for other confining stresses.

It has been suggested that the crack-damage stress is defined by sliding since the axial strain registers permanent damage. This would imply that the crack-damage locus is the locus of strength required to initiate crack sliding or simply the Griffith locus, as defined by Cook [33]. Only a brief summary of Cook's original work is provided, and the interested reader is referred to Cook's paper for the derivation of the formulas that follow. For the confined case, consider a single elliptical crack of length $2c$, inclined at some angle θ to the direction of the applied stress σ_1, in a specimen where n represents the number of cracks per unit volume (see Fig. 13). Using the approach of Cook the critical axial strain ϵ_{cr}, at which sliding occurs, is given by

$$\epsilon_{cr} = \frac{\sigma_1 - 2\nu\sigma_3}{2G(1+\nu)} + \frac{2}{(\sigma_1 - \sigma_3)}\left(W_s + \frac{W_f}{2}\right)n \tag{4}$$

where

$$W_s = \frac{\pi}{4}(1-\nu)\frac{(\tau - \mu\sigma_n)^2}{G}c^2$$

$$W_f = \frac{\pi}{2}(1-\nu)\mu\sigma_n\frac{(\tau - \mu\sigma_n)}{G}c^2$$

$$c = \frac{8\alpha G}{\pi(1-\nu)(\tau - \mu\sigma_n)^2}$$

and where ν is the Poisson's ratio, G is the modulus of rigidity, μ is the friction across crack faces, τ is the shear stress in the direction of the crack slip, σ_n is the normal stress acting on the surface of the crack, and α is the fracture surface energy.

For the conditions of triaxial compression and assuming that the crack is parallel to the direction of the intermediate compressive stress

$$\sigma_n = \frac{\sigma_1 + \sigma_3}{2} - \frac{\sigma_1 - \sigma_3}{2}\cos 2\theta$$

$$\tau = \frac{\sigma_1 - \sigma_3}{2}\sin 2\theta \tag{5}$$

where θ is the angle between the critical crack surface and the direction of the maximum applied stress, σ_1.

Hence ϵ_{cr} can be obtained provided the crack density n and the fracture surface energy α are known. The other parameters are available from standard laboratory tests and the fracture surface energy can be equated to the strain energy release rate $\mathcal{G}$ by $\mathcal{G} = 2\alpha$. The strain energy release rate is one of the most important parameters,

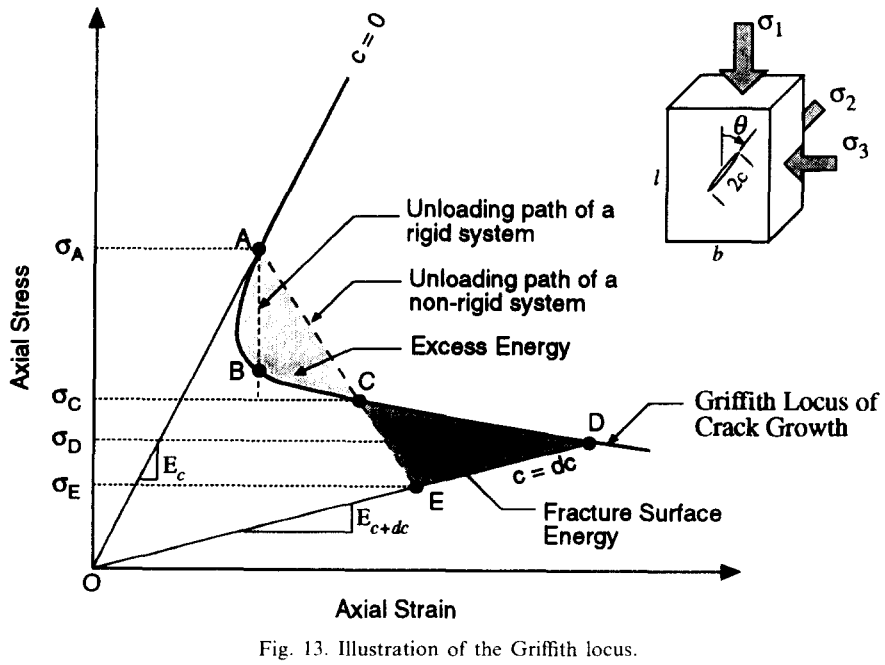

Fig. 13. Illustration of the Griffith locus.

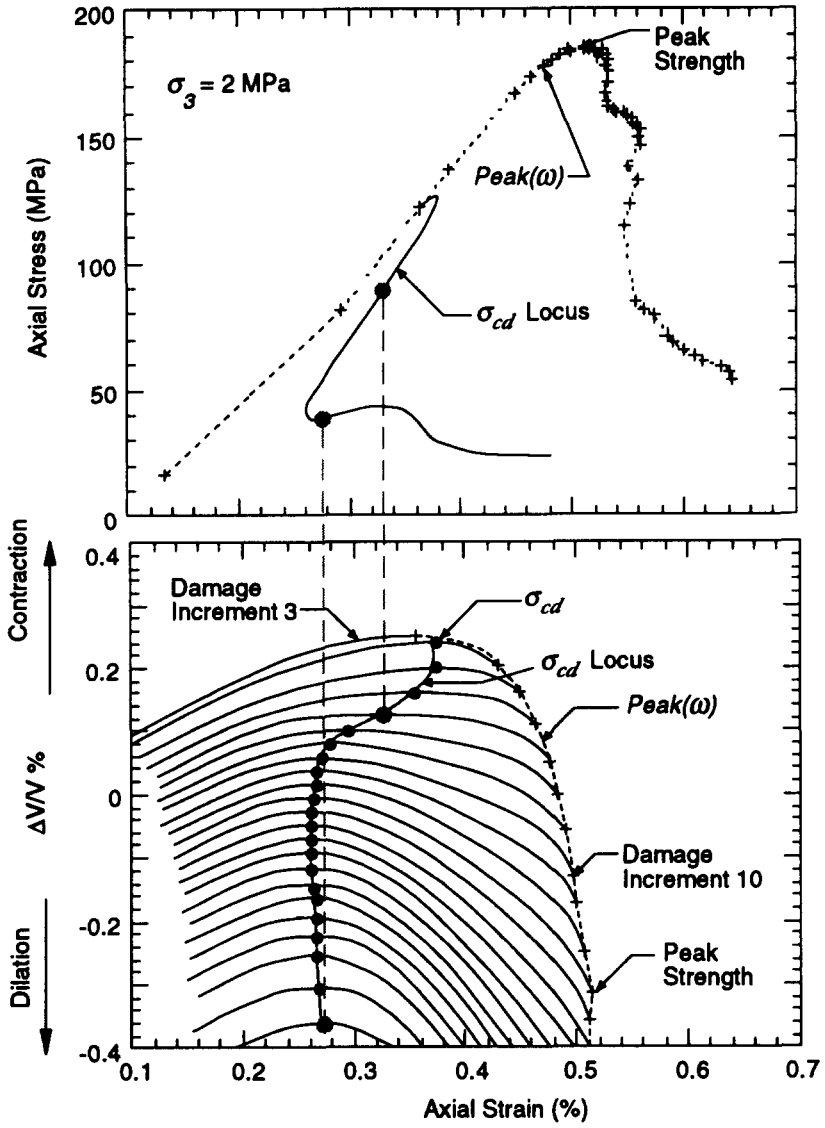

Fig. 14. Crack-damage locus and peak strength versus axial strain. The volumetric strain for each damage increment is also shown. Note that the major drop in the crack-damage locus occurs before the peak strength is reached.

with regard to fracture, and is defined as the amount of energy release per unit increase in crack surface area. Rice [34] proposed a method for determining $\mathcal{G}_c$, the strain energy release rate at failure, for shear faulting. Using Rice's approach, Kemeny and Cook [35] calculated a $\mathcal{G}_c$ value of 1.05 J/m^2 for the creation of a single shear fault for Westerly granite. Since $\mathcal{G}_c$ is considered to be a material property, the value determined by Kemeny and Cook will be used as a starting point in evaluating the model for Lac du Bonnet granite.

To calibrate the model for the crack density n, the critical axial strains were fitted to the data from an unconfined test to estimate a value for n. All other input parameters were taken from laboratory test results and used to predict the critical strain at confining stresses of 2, 15 and 30 MPa. The predicted values were compared with the measured crack-damage locus at these confining stresses (Fig. 15). It should be noted that the non-linear strains that occurred in the initial seating phase of the test were added to the calculated results in order to compare with the measured strains. The parameters used in equation (4) are shown in Fig. 15. It should be noted that in Fig. 15, the initial positive slope of the locus is somewhat less than that of the measured values at the higher confining stresses and the discrepancy increases with confining pressure. This occurs because no correction for the increasing stiffness (E) of the samples with confining stress was made. Because of the high density of microcracks in the samples, Young's modulus increases from about 50 GPa for the unconfined samples to about 60 GPa for the 30 MPa confining stress. Even without this correction, the agreement between the measured and the predicted loci is quite good.

According to Cook, the critical condition for the initiation of failure occurs when

$$\frac{\pi}{2}(1-\nu)\frac{(\tau-\mu\sigma_n)^2}{G}c \geqslant 4\alpha. \tag{6}$$

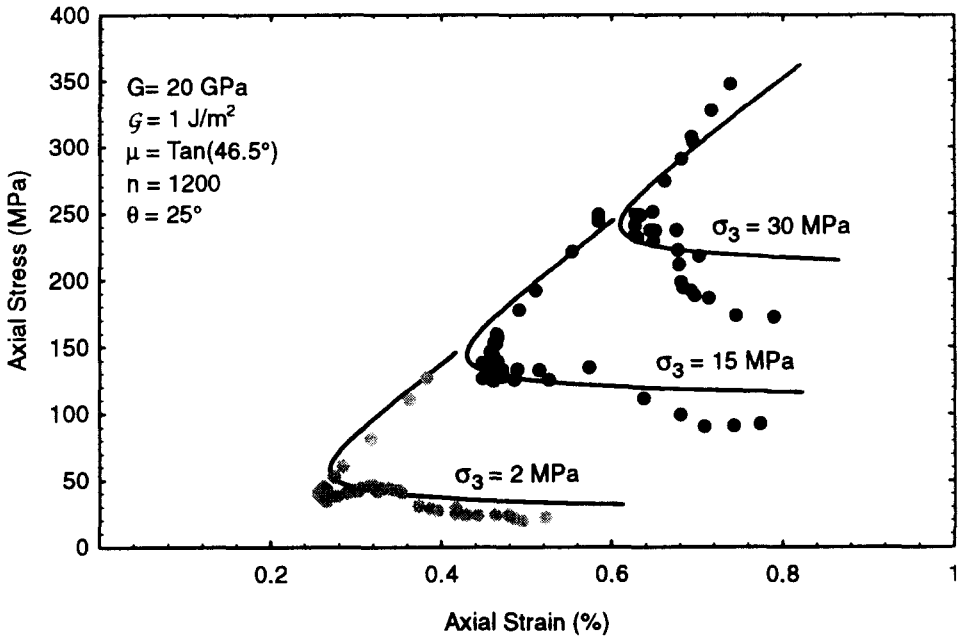

Fig. 15. Crack-damage locus at various confining stresses.

Substituting equation (5) into equation (6) provides the strength of the specimen in a general Mohr–Coulomb form:

$$\sigma_1 \geqslant \frac{\sqrt{\dfrac{8\alpha G}{c\pi(1-\nu)}}}{\sin\theta\cos\theta(1-\mu\tan\theta)} + \sigma_3 \frac{\left(1+\dfrac{\mu}{\tan\theta}\right)}{1-\mu\tan\theta}. \quad (7)$$

Note that the critical angle of θ will be related to μ in order that $(\tau - \mu\sigma_n)$ in equation (6) is a maximum when

$$\theta_{\text{critical}} = \frac{1}{2}\tan^{-1}\frac{1}{\mu}.$$

Thus equation (7) can be rewritten as

$$\sigma_1 \geqslant \frac{\sqrt{\dfrac{8\alpha G}{c\pi(1-\nu)}}}{\sqrt{1+\mu^2}-\mu} + \sigma_3\left(\frac{\sqrt{1+\mu^2}+\mu}{\sqrt{1+\mu^2}-\mu}\right) \quad (8)$$

It was stated previously that the crack-damage loci were similar in shape regardless of confining stress. Figure 16 shows typical examples of the crack-damage locus for some of the confining stresses tested. Not all of the results are shown in this figure for clarity reasons, however all of the results are shown in Fig. 17. The condition for sliding, according to equation (6) is a linear relationship in σ_1–σ_3 space. The crack-damage threshold

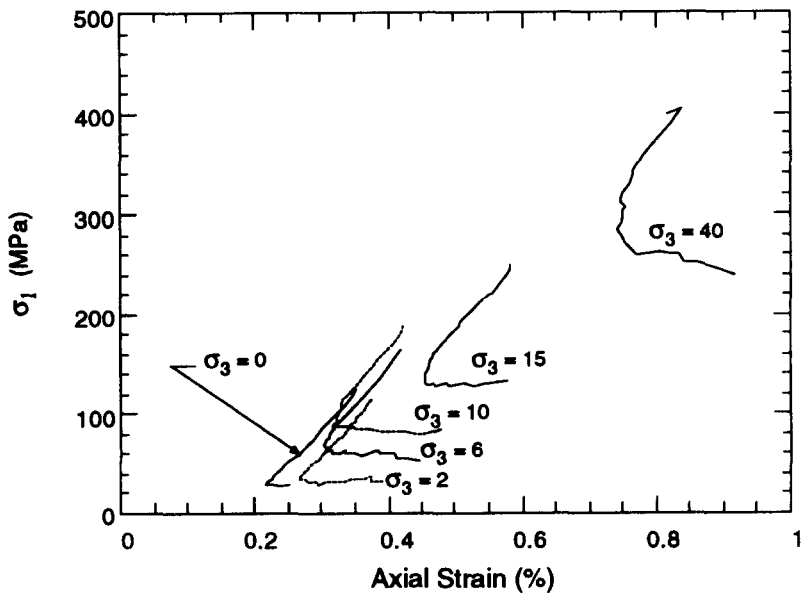

Fig. 16. Crack-damage locus at various confining stresses.

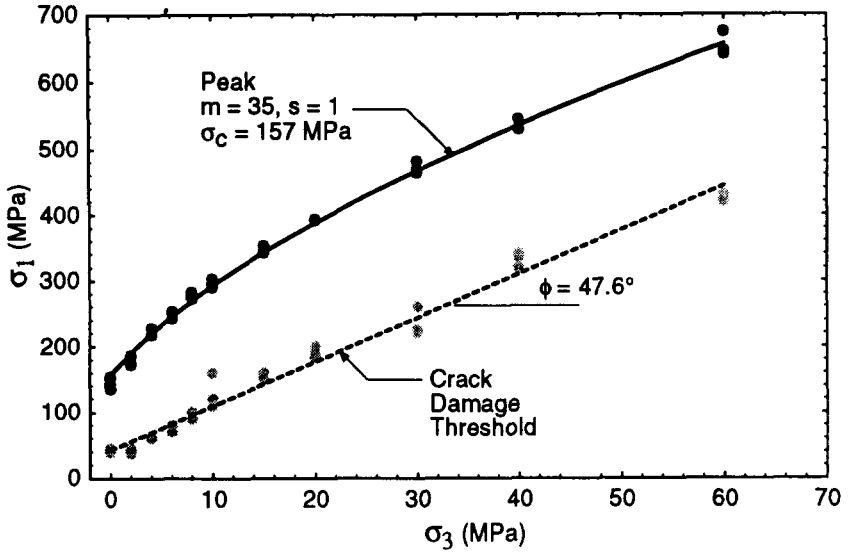

Fig. 17. The peak strength and crack-damage threshold failure envelopes.

values also follow a linear relationship in σ_1–σ_3 space, which gives a friction angle of 47.6°. This friction value is close to the residual friction angle of 45° reported by Gyenge *et al.* [36] and 42–43° reported by Lajtai and Gadi [37] for Lac du Bonnet granite (Fig. 18). The peak strength is also shown in Fig. 17 with a Hoek–Brown failure envelope fitted to the data.

DISCUSSION

Coulomb (1796) [38] postulated that the shear strength of rock and of soil is made up of two components—a constant cohesion, and a normal stress-dependent frictional component. Schmertmann and Osterberg [39] showed that for clays these components are not mobilized at the same displacements. However, for rock engineering design purposes, it is generally assumed that these components are mobilized at the same displacements such that both components can be relied on simultaneously in rock engineering design. The strength of intact rock is determined in the laboratory using triaxial tests, and the cohesion and friction components are combined in the strength value obtained from any one test. The Griffith locus can be used to determine the relationship between cohesion and friction during the failure process.

The shear criterion given in equation (8) can be reduced to

$$\sigma_1 = 2\sqrt{\frac{2\alpha G}{c\pi(1-\nu)}}\tan\left(45+\frac{\phi}{2}\right)+\sigma_3\tan^2\left(45+\frac{\phi}{2}\right) \quad (9)$$

by substituting $\mu = \tan\phi$, where ϕ is the friction angle.

The shear strength of a frictional material is also given by the well-known Mohr–Coulomb criterion

$$\sigma_1 = 2S_0\tan\left(45+\frac{\phi}{2}\right)+\sigma_3\tan^2\left(45+\frac{\phi}{2}\right) \quad (10)$$

where S_0 is the empirical cohesion intercept or intrinsic strength. It is interesting to note that the two shear criteria in equations (9) and (10) are identical. In equation (9) the empirical cohesion of equation (10) is expressed in terms of fracture surface energy and crack length. More importantly, an examination of equations (9) and (10) reveals that the fracture surface energy and

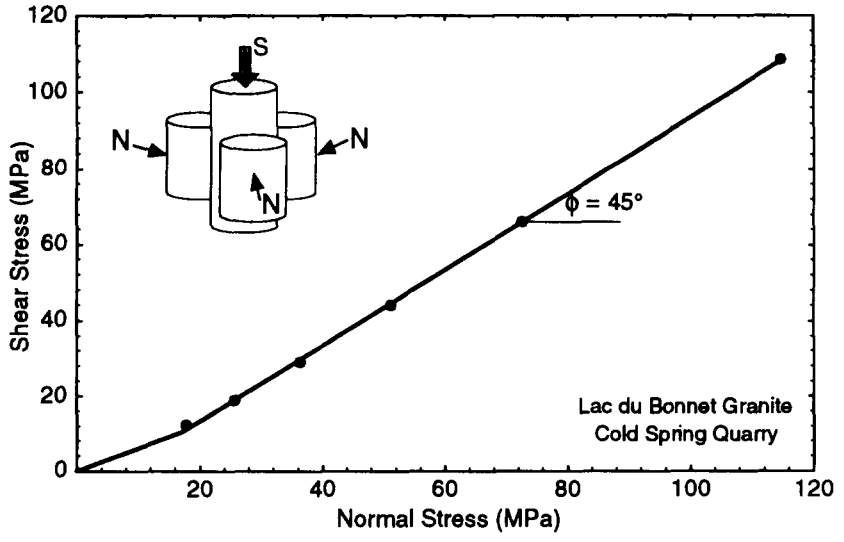

Fig. 18. Basic friction for Lac du Bonnet granite, after Gyenge *et al.* [36],

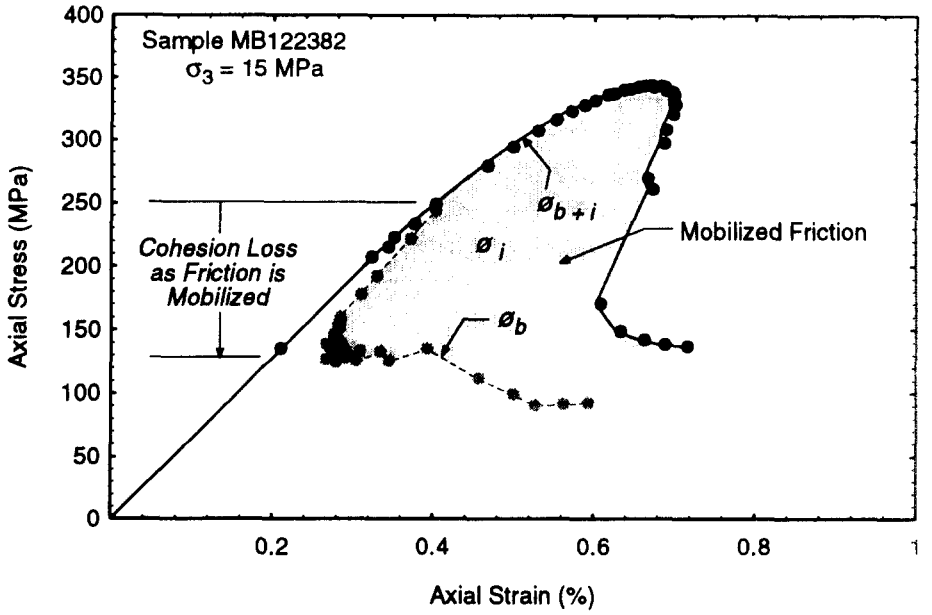

Fig. 19. Mobilization of friction and cohesion as a function of axial strain.

crack length only apply to the cohesive component of the material and that the frictional strength is not dependent on these parameters.

The interpretation of a standard set of uniaxial test results, using equation (10) would imply that

$$\sigma_1 = 2S_0 \tan\left(45 + \frac{\phi}{2}\right). \tag{11}$$

Thus the cohesion can be equated to the strength just as sliding starts, which for our tests results is the crack-damage stress. For an unconfined test, at the instant when sliding starts, the cohesion becomes

$$2S_0 = \sigma_{cd}.$$

Once sliding initiates, i.e. friction is being mobilized, the strength of the sample starts to increase above the crack-damage stress. However, we have seen from our test results that as the sample is subjected to increasing damage, only a small amount of damage to the sample is necessary to bring the crack-damage stress to the threshold value, suggesting that cohesion must also decrease. The total strength of the sample has not changed, therefore the frictional component of equation (11) must be increasing as the cohesion is decreasing. In equation (9) the drop in cohesion is related to an increase in crack length. Figure 19 presents an example of this progressive fracturing, illustrating the loss in cohesion and the mobilization of friction, and Fig. 20 illustrates the concept in terms of a Mohr stress diagram. Ultimately, in Fig. 19, at large displacements, the peak stress and the crack damage stress should be equal.

This concept of cohesion loss can only be explained in this manner if non-elastic deformations are required to mobilize friction and if the frictional component is made up of a residual component (ϕ_b) and a roughness of interlocking component (ϕ_i), such that the total frictional residence can be expressed as ϕ_{b+i}. The interlocking decreases from a maximum as damage accumulates and as friction is mobilized, the residual friction and the minimum cohesion must be approaches (see Fig. 21). For Fig. 21, the value of ϕ was calculated using

$$\phi = 2\tan^{-1}\left(\frac{\sigma_1}{\sigma_{cd}}\right) - \frac{\pi}{2}.$$

Furthermore in Fig. 21, the damage has been normalized with respect to the value of ω at the end of the test and the strength has been normalized to the peak strength. Figure 21 illustrates that the peak friction angle ($\phi_{b+i} = 63°$) is only reached when most of the cohesion is lost. With increasing damage, the friction angle gradually decreases to about 42°. This friction value is similar

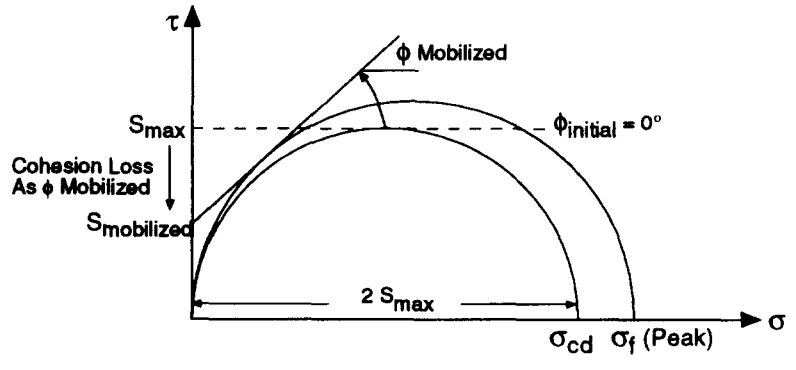

Fig. 20. Illustration of cohesion loss and mobilization of friction in terms of Mohr stress diagram.

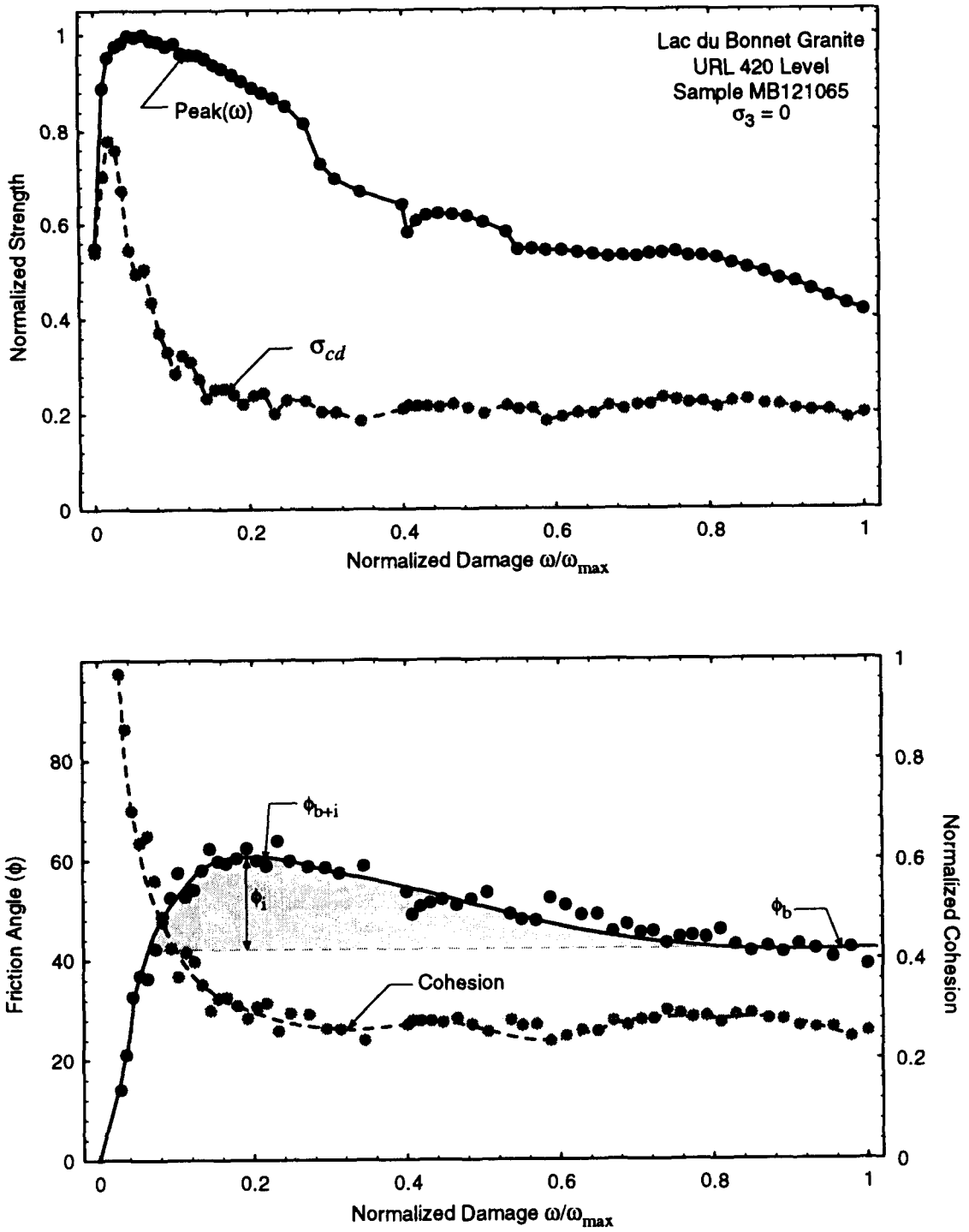

Fig. 21. Mobilization of friction and cohesion as a function of normalized damage.

to the residual friction angle of 42–45° for Lac du Bonnet granite reported by [36,37]. Thus for the test presented in Fig. 21, it appears that the residual friction is nearly reached. The peak friction angle of 63°, although high, is not unrealistic, e.g. Dusseault and Morgenstern [40] reported that natural slopes of uncemented locked sands have inclinations greater then 54°. Thus 63° does not seem unreasonable for perfectly interlocked mineral grains subjected to small displacements.

Application of the Griffith locus

The Griffith crack-damage locus can be readily applied to the rock surrounding an underground opening. As the face of the opening approaches and passes the volume of rock that eventually becomes part of the tunnel surface, the principal stresses associated with this rock will change significantly in both magnitude and direction. Stress concentrations in excess of the crack-damage locus, occurring at any period in the rocks loading history around the opening, will result in a localized increase of damage to the rock and a corresponding loss of cohesion. The degree of damage will be highest at the surface of the opening where confinement is zero and stress concentrations are greatest, and this damage will decrease with increasing distance into the rock. From equations (9) or (10), it can be seen that

when $\sigma_3 = 0$, the frictional component of the rock's strength plays essentially no role in determining the strength around an underground opening. The strength is determined by the cohesion which is a function of crack damage. Hence the strength around an underground opening, in a high stress environment, will be lowest at the tunnel surface. For this class of problems back analysis of the failed or damaged openings to determine the *in situ* strength would suggest much lower strength than that found from routine laboratory testing, even if the rock mass was fairly massive. For our test results, the cohesion loss was greater than 50% of laboratory unconfined compressive strength. This low-strength material would only be present in the local area around the tunnel that has experienced the damage, and the rock mass outside this damaged zone would still have the undamaged strength. This may be one of the contributing factors to restricting the depth of borehole-breakouts, or failure zones around deep tunnels and may also help explain an observed phenomenon that the back-analysed strength around tunnels with stress-induced failures is about half the measured unconfined compressive strength [41,42,43,44].

CONCLUSIONS

The progressive failure of Lac du Bonnet granite was investigated by damage-controlled testing of 6 uniaxial and 33 triaxial samples. The testing was carried out to investigate the influence of crack damage on the crack-damage stress (σ_{cd}) and the crack-initiation stress (σ_{ci}). The results demonstrated that the crack-initiation stress remains fairly constant and is independent of the damage accumulated in the sample. The crack-damage stress however is very dependent on the amount of accumulated damage. It is proposed that as the granite is loaded in compression to its crack-damage stress, its strength is derived only from cohesion. When the load exceeds its cohesive strength, which occurs at about 0.7–0.85 of the peak compressive strength, damage occurs. As the Lac du Bonet granite is damaged, a portion of its cohesive strength component is lost, and friction is mobilized. The loss in cohesion can be traced using the crack-damage locus. For small amounts of damage, this cohesion loss can amount to 50% or more of the initial cohesion. Friction is mobilized as the cohesion is lost and reaches a peak value (63° for the unconfined sample) when damage to the sample is small. As damage increases, the friction angle decreases, trending towards a residual value of about 45°.

The crack-damage stress was modelled using the Griffith locus based on a sliding crack. The predicted locus agreed very closely with the measured crack-damage locus obtained from the damage-controlled tests. The failure enveloped based on the Griffith locus is of the same general form as Mohr–Coulomb, and the failure strength from the measured crack-damage locus, in the damage-controlled laboratory tests, is also linear.

The laboratory results indicate that if a brittle material is damaged, the unconfined strength is reduced and this reduction is a function of the accumulated damage. Hence the strength around an unconfined underground opening, in a high stress environment, will be lowest at the tunnel surface. Thus back analysis of the failed or damaged openings to determine the *in situ* strength would suggest much lower strength than that found from routine laboratory testing, even if the rock mass was fairly massive. This low-strength damaged material would be localized around the opening, and the rock mass outside this damaged zone would still have the undamaged strength. It is suggested that this may be one of the contributing factors to restricting the depth of borehole-breakouts, or failure zones, around deep tunnels and may also help explain an observed phenomenon that the back-analysed strength around tunnels with stress-induced failures is about half the measured unconfined compressive strength.

Acknowledgements—This work was supported by the Canadian Nuclear Fuel Waste Management Program which is jointly funded by AECL and Ontario Hydro under the auspices of the Candu Owners Group.

Accepted for publication 22 April 1994.

REFERENCES

1. Morgenstern N. R. Progressive failure in theory and practice: 28th Terzaghi Lecture. *ASCE Jl Geotech. Envir. Engng.* In preparation.
2. Brown E. T. (Ed.) *Rock Characterization Testing and Monitoring, ISRM Suggested Methods*. pp. 107–127. Pergamon Press, Oxford (1981).
3. Richart F. E., Brandtzaeg A. and Brown R. L. A study of the failure of concrete under combined compressive stresses. Bulletin 128, University of Illinois Engineering Experiment Station (1928).
4. Cook N. G. W. An experiment proving that dilatancy is a pervasive volumetric property of brittle rocks loaded to failure. *Rock Mech. Rock Engng* **2**, 181–188 (1970).
5. Hoek E. and Bieniawski Z. T. Brittle fracture propagation in rock under compression. *J. Fracture Mech.* **1**, 137–155 (1965).
6. Brace W. F., Paulding B. and Scholz C. Dilatancy in the fracture of crystalline rocks. *J. Geophys. Res.* **71**, 3939–3953 (1966).
7. Bieniawski Z. T. Mechanism of brittle fracture of rock, parts I, II and III. *Int. J. Rock Mech. Min. Sci. & Geomech. Abstr.* **4**, 395–430 (1967).
8. Brace W. F. and Byerlee J. D. Recent experimental studies of brittle fracture of rocks. In *Proc. 8th U.S. Symp. on Rock Mechanics, Minneapolis* (Edited by Fairhurst C.), pp. 58–81. American Institute of Mining Engineers (1968).
9. Scholz C. H. Experimental study of the fracturing process in brittle rocks. *J. Geophys. Res.* **73**, 1447–1453 (1968).
10. Wawersik W. R. and Fairhurst C. A study of brittle rock fracture in laboratory compression experiments. *Int. J. Rock Mech. Min. Sci. & Geomech. Abstr.* **7**, 561–575 (1970).
11. Wawersik W. R. and Brace W. F. Post failure behaviour of a granite and diabase. *Rock Mech. Rock Engng* **3**, 61–85 (1971).
12. Peng S. S. and Johnson A. M. Crack Growth and faulting in cylindrical specimens of Chelmsford granite. *Int. J. Rock Mech. Min. Sci. & Geomech. Abstr.* **9**, 37–86 (1972).
13. Hallbauer D. K., Wagner H. and Cook N. G. W. Some observations concerning the microscopic and mechanical behaviour of quartzite specimens in stiff, triaxial compression tests. *Int. J. Rock Mech. Min. Sci. & Geomech. Abstr.* **10**, 713–726 (1973).
14. Tapponnier P. and Brace W. F. Development of stress-induced microcracks in Westerly granite. *Int. J. Rock Mech. Min. Sci. & Geomech. Abstr.* **13**, 103–112 (1976).
15. Haimson B. C. and Kim C. M. Mechanical behaviour of rock under cyclic fatigue. In *Proc. 13th U.S. Symp. on Rock Mechanics, University of Illinois* (Edited by Cording E. J.), pp. 373–378. American Society of Civil Engineers, New York (1972).
16. Rusch H. Physical problems in the testing of concrete. Zement-Kalk-Gips (Cement and Concrete Association Library Translation No. 86, 1960), pp. 1–9 (1959).

17. Rusch H. Research towards a general flexural theory for structural concrete. *Proc. Am. Concrete Inst.* **57,** 1–28 (1960).
18. Munday J. G. L. and Dhir R. K. Long-term strength of concrete under sustained load. In *Proc. 2nd Australian Conference on Engineering Materials*, Sydney, Australia, pp. 109–120. University of NSW, Australia (1981).
19. Lajtai E. Z., Carter B. J. and Duncan E. J. S. Mapping the state of fracture around cavities. *Engng Geol.* **31,** 277–289 (1991).
20. Schmidtke R. H. and Lajtai E. The long-term strength of Lac du Bonnet granite. *Int. J. Rock Mech. Min. Sci. & Geomech. Abstr.* **22,** 461–465 (1985).
21. Lockner D. A., Byerlee J. D., Kuksenko V., Ponomarev A. and Sidorin A. Quasi-static fault growth and shear fracture energy in granite. *Nature* **350,** 39–42 (1991).
22. Hudson J. A., Brown E. T. and Fairhurst C. Shape of the complete stress–strain curve for rock. In *Proc. 13th U.S. Symp. on Rock Mechanics, Urbana* (Edited by Cording E. J.), pp. 773–795. American Society of Civil Engineers, New York (1972).
23. Glucklich J. and Cohen L. J. Size as a factor in the brittle–ductile transition and the strength of some materials. *Int. J. Fracture Mech.* **3,** 278–289 (1967).
24. Glucklich J. and Cohen L. J. Strain energy and size effects in a brittle material. *Mater. Res. Standards* **8,** 17–22 (1968).
25. Krempl E. Models of viscoplasticity—some comments on equilibrium (back) stress and drag stress. *Acta Mech.* **69,** 25–42 (1987).
26. Hoek E. and Brown E. T. *Underground Excavations in Rock*. The Institution of Mining and Metallurgy, London (1980).
27. Lau J. S. O. and Gorski B. The post failure behaviour of Lac du Bonnet grey granite. Divisional Report MRL 91-079(TR), CANMET, Energy Mines and Resources, Canada (1991).
28. Saint-Leu C. and Sirieys P. La fatigue des roches. In *Proc. Int. Symp. on Rock Mechanics*, Vol. 1, pp. II–18. (1971).
29. Scholz C. H. and Kranz R. Notes on dilatancy recovery. *J. Geophys. Res.* **79,** 2132–2135 (1974).
30. Haimson B. C. Mechanical behaviour of rock under cyclic loading. In *Proc. 3rd Congress Int. Soc. Rock Mech.*, Denver, Vol. II, pp.1 373–379. National Academy of Sciences, Washington, DC (1974).
31. Berry J. P. Some kinetic considerations of the Griffith criterion for fracture I: equations of motion at constant force. *J. Mech. Phys. Solids* **8,** 194–206 (1960).
32. Berry J. P. Some kinetic considerations of the Griffith criterion for fracture II: equations of motion at constant deformation. *J. Mech. Phys. Solids* **8,** 207–216 (1960).
33. Cook N. G. W. The failure of rock. *Int. J. Rock Mech. Min. Sci. & Geomech. Abstr.* **2,** 389–403 (1965).
34. Rice J. R. The mechanics of earthquake rupture. In *Proc. Int. School of Physics, Course LXXVIII, Physics of the Earth's Interior* (Edited by Dziewonski A. M. and Boschi E.), pp. 555–649. North–Holland, Amsterdam (1980).
35. Kemeny J. M. and Cook N. G. W. Determination of rock fracture parameters from crack models for failure in compression. In *Proc. 28th U.S. Symp. on Rock Mechanics, Tuscon* (Edited by Desai C. S., Krempl E., Kiousis P. D. and Kundu T.), pp. 367–375. Balkema, Rotterdam (1987).
36. Gyenge M., Jackson R. and Gorski B. Residual strength envelopes using the confined shear test method. In *Proc. 32th U.S. Symp. on Rock Mechanics, Norman* (Edited by Roegiers J.-C.), pp. 629–635. Balkema, Rotterdam (1991).
37. Lajtai E. Z. and Gadi A. M. Friction on a granite to granite interface. *Rock Mech. Rock Engng* **22,** 25–49 (1989).
38. Brady B. H. G. and Brown E. T. *Rock Mechanics for Underground Mining*, 1st Edn. Allen & Unwin, London (1985).
39. Schmertmann J. H. and Osterberg J. O. An experimental study of the development of cohesion and friction with axial strain in saturated cohesive soils. In *Research Conference on Shear Strength of Cohesive Soils*, Boulder, Colo, pp. 643-694. American Society for Civil Engineers, New York (1960).
40. Dusseault M. B. and Morgenstern N. R. Locked sands. *Q. J. Engng Geol.* **12,** 117–131 (1979).
41. Pelli F., Kaiser P. K. and Morgenstern N. R. An interpretation of ground movements recorded during construction of the Donkin–Morien tunnel. *Can Geotech. J.* **28,** 239–254 (1991).
42. Stacey T. R. A simple extension strain criterion for fracture of brittle rock. *Int. J. Rock Mech. Min. Sci. & Geomech. Abstr.* **18,** 469–474 (1981).
43. Myrvang A. M. Estimation of *in situ* compressive strength of rocks from *in situ* stress measurements in highly stressed rock structures. In *Proc. 7th ISRM Congress on Rock Mechanics, Aachen* (Edited by Wittke W.), pp. 573–575. Balkema, Rotterdam (1991).
44. Herget G. *Stresses in Rock*. Balkema, Rotterdam (1988).